Structural toggle in the RNaseH domain of Prp8 helps balance splicing fidelity and catalytic efficiency

Megan Mayerle[a,1], Madhura Raghavan[b,1], Sarah Ledoux[a,1], Argenta Price[a,1,2], Nicholas Stepankiw[b], Haralambos Hadjivassiliou[a], Erica A. Moehle[a,3], Senén D. Mendoza[a], Jeffrey A. Pleiss[b,4], Christine Guthrie[a,4], and John Abelson[a,4]

[a]Department of Biochemistry and Biophysics, University of California, San Francisco, CA 94143; and [b]Department of Molecular Biology and Genetics, Cornell University, Ithaca, NY 14853

Contributed by John Abelson, March 22, 2017 (sent for review January 26, 2017; reviewed by Harry F. Noller and Joan A. Steitz)

Pre-mRNA splicing is an essential step of eukaryotic gene expression that requires both high efficiency and high fidelity. Prp8 has long been considered the "master regulator" of the spliceosome, the molecular machine that executes pre-mRNA splicing. Cross-linking and structural studies place the RNaseH domain (RH) of Prp8 near the spliceosome's catalytic core and demonstrate that *prp8* alleles that map to a 17-aa extension in RH stabilize it in one of two mutually exclusive structures, the biological relevance of which are unknown. We performed an extensive characterization of *prp8* alleles that map to this extension and, using in vitro and in vivo reporter assays, show they fall into two functional classes associated with the two structures: those that promote error-prone/efficient splicing and those that promote hyperaccurate/inefficient splicing. Identification of global locations of endogenous splice-site activation by lariat sequencing confirms the fidelity effects seen in our reporter assays. Furthermore, we show that error-prone/efficient RH alleles suppress a *prp2* mutant deficient at promoting the first catalytic step of splicing, whereas hyperaccurate/inefficient RH alleles exhibit synthetic sickness. Together our data indicate that *prp8* RH alleles link splicing fidelity with catalytic efficiency by biasing the relative stabilities of distinct spliceosome conformations. We hypothesize that the spliceosome "toggles" between such error-prone/efficient and hyperaccurate/inefficient conformations during the splicing cycle to regulate splicing fidelity.

spliceosome | Prp8 | splicing fidelity | splicing efficiency | lariat sequencing

Pre-mRNA splicing occurs via two transesterification reactions catalyzed by the spliceosome, a large, dynamic ribonucleoprotein complex. The catalytically active spliceosome is composed of three small nuclear ribonucleoprotein (snRNP) complexes (U2, U5, and U6), the Nineteen Complex and its related proteins, and a small number of accessory splicing proteins (1). In the first catalytic step of pre-mRNA splicing the 5′ splice site (5′SS) is cleaved, forming a lariat-3′ exon intermediate in which the 5′SS is covalently linked via a 2′,5′ phosphodiester bond to the branch site adenosine (BrA). In the second catalytic step the 3′ splice site (3′SS) is cleaved and the 5′ and 3′ exons are ligated. The excised lariat intron is then released from the spliceosome. Splicing is performed with high fidelity and high efficiency, and it is thought that core spliceosomal components contribute directly to maintenance of splicing fidelity and efficiency (1, 2).

Prp8 is the largest and most highly conserved protein in the spliceosome and is a component of the U5 snRNP. Recent cryoelectron microscopy structures show that Prp8 acts as a platform at the heart of the spliceosome and undergoes considerable conformational rearrangements during the splicing cycle (3–11). Genetic screens have identified many alleles in Prp8 that exhibit compromised splicing fidelity or efficiency (summarized in ref. 12). A subset of these mutations maps to a unique and essential 17-aa extension within the RNaseH domain (RH) of Prp8 (13–20). Structural studies reveal that the RH extension can exist either in a β-hairpin form or as a disordered loop, and that it adopts these conformations at distinct steps of the splicing cycle (Fig. 1) (3, 4, 7–11, 19). Of the subset of *prp8* alleles that map to the RH extension for which structural data are available, those that preferentially stabilize either the β-hairpin or disordered loop forms of RH correlate with distinct genetic phenotypes previously proposed to arise from unique first-step and second-step catalytic conformations of the spliceosome (Fig. 1 and Table S1) (17–20).

However, recent structural and biochemical studies of the spliceosome and its evolutionary precursor, the group II intron, reveal that the spliceosome's catalytic core is similar at both catalytic steps (21, 22). Structural data further suggest the group II intron passes through an obligatory intermediate transitional structure between two highly similar first- and second-step catalytic structures (22). Conservation argues that some components of the spliceosome might adopt a similar transitional intermediate, "toggling" between catalytic and transitional intermediate conformations during a typical splicing reaction, and that these conformations would be executed through specific structural toggles in core spliceosomal components (17).

Here we provide evidence for two distinct classes of *prp8* RH alleles, which we refer to as "catalytic" and "transitional" in keeping with the nomenclature established for the group II intron. Specifically, catalytic *prp8* alleles that stabilize the loop structure of the RH extension exhibit high-efficiency, low-fidelity splicing, whereas transitional *prp8* alleles that stabilize the β-hairpin structure exhibit low-efficiency but high-fidelity splicing both on reporter constructs

Significance

The spliceosome, which catalyzes pre-mRNA splicing via a two-step process, must balance the need for high-fidelity splice-site selection with the need for rapid, efficient splicing. We propose that the RNaseH domain (RH) of Prp8 contributes to this balance by toggling between two different conformations throughout the splicing cycle. Using a set of previously published *prp8* alleles, we link alleles that stabilize one conformation of RH to high-fidelity, low-efficiency splicing and those that stabilize the other to low-fidelity, high-efficiency splicing. This model is consistent with recent data that indicate the conformation of the spliceosome is similar at both catalytic steps and provides an example of a structural basis for splicing fidelity.

Author contributions: M.M., M.R., S.L., A.P., N.S., H.H., J.A.P., C.G., and J.A. designed research; M.M., M.R., S.L., A.P., N.S., H.H., E.A.M., and S.D.M. performed research; M.M., M.R., S.L., A.P., N.S., and H.H. contributed new reagents/analytic tools; M.M., M.R., S.L., A.P., N.S., S.D.M., J.A.P., C.G., and J.A. analyzed data; and M.M., M.R., S.L., A.P., J.A.P., C.G., and J.A. wrote the paper.

Reviewers: H.F.N., University of California, Santa Cruz; and J.A.S., Howard Hughes Medical Institute, Yale University.

The authors declare no conflict of interest.

Data deposition: The sequences reported in this paper have been deposited in the NCBI GEO database (accession no. GSE96891).

[1]M.M., M.R., S.L., and A.P. contributed equally to this work.

[2]Present address: Department of Physics, University of Colorado, Boulder, CO 80309.

[3]Present address: Department of Molecular and Cell Biology, University of California, Berkeley, CA 94720.

[4]To whom correspondence may be addressed. Email: jpleiss@gmail.com, christineguthrie@gmail.com, or johnabelson@gmail.com.

This article contains supporting information online at www.pnas.org/lookup/suppl/doi:10.1073/pnas.1701462114/-/DCSupplemental.

GENETICS

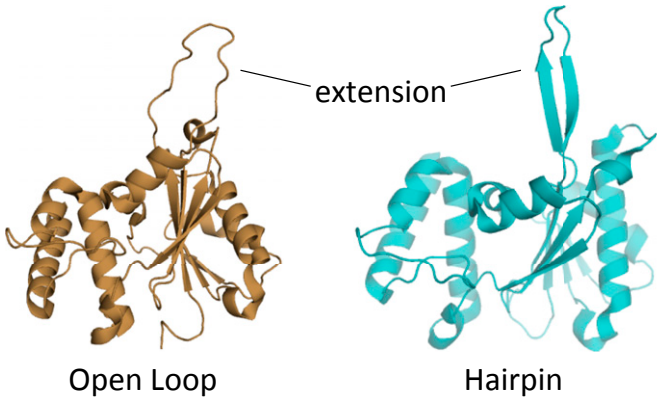

Fig. 1. The 17-aa extension in the RNaseH subdomain of Prp8 adopts two different forms: an open loop (tan, *Left*) and a β-hairpin (cyan, *Right*). Structures are modified from Protein Data Bank ID code 4JK7 (19).

and at endogenous splice sites genomewide. We propose that the spliceosome cycles between catalytic and transitional conformations during each splicing cycle, and we implicate the RH extension of Prp8 as a structural toggle. This model is supported by recent high-resolution structural studies of the spliceosome that show that the RH extension adopts a loop form in the catalytically active B^{act} spliceosome (5) and a β-hairpin form in other noncatalytically active conformations (3, 4, 7–9). Our data provide a specific, mechanistic example of how distinct conformations of a core spliceosomal component can affect both splicing fidelity and efficiency.

Results

Creation of *prp8* Toggle Allele Strains. We chose 13 published *prp8* RH extension alleles for characterization: V1860D, V1860N, T1861P, V1862D, V1862Y, H1863E, K1864E, T1865K, N1869D, V1870N, A1871E, T1872E, and I1875T. Together, we refer to these alleles as the "toggle" alleles. Whereas most of these alleles were discovered through genetic screens conducted to identify alleles that suppress growth defects caused by the mutation of the 5′SS, branch point (Br), or 3′SS motifs of a reporter gene (16–18, 20, 23), a subset was deliberately designed based on structural data (13) (Table S1). Structural data are available for a subset of these alleles (19); for the other alleles, we made predictions based on the available data (Table S1). Most alleles grew similarly to WT yeast in rich media at all temperatures tested, consistent with previous results. A strain in which the entire 17-aa RH extension was deleted failed to grow at any temperature (Table S1).

***ACT1-CUP1* Reporter Assay Demonstrates That *prp8* Toggle Alleles Sort into Two Distinct Classes.** To determine the effects of the *prp8* toggle alleles on splicing fidelity and efficiency we used the well-characterized *ACT1-CUP1* splicing reporter system (Fig. 2*A* and Table S2) (24). In this system, the ability of yeast to grow on otherwise lethal concentrations of copper-containing media is directly proportional to splicing efficiency. *ACT1-CUP1* reporters containing nonconsensus splicing sequences at the 5′SS (G1A, U2A, and G5A), Br (C256A, BrC, and BrG), or 3′SS (U301G, A302G, and G303/304C) were used to measure fidelity (Fig. 2 *B* and *C*). A false-color representation of the data is shown in Fig. 2*D* (25), and the results are consistent with reported data for the subset of toggle alleles previously examined (Fig. S1) (13, 16–20).

All *prp8* toggle alleles grew with efficiency similar to *PRP8* when required to splice a WT *ACT1-CUP1* reporter. However, individual *prp8* toggle alleles exhibited differential growth on *ACT1-CUP1* reporters with mutated, nonconsensus splicing sequences (Fig. 2*D* and Fig. S1). In general, *prp8* toggle alleles sorted into two groups: those that exhibited worse growth (blue, Fig. 2*D*) than *PRP8* (indicative of hyperaccurate/inefficient splicing) and those that exhibited better growth (indicative of error-prone splicing) (yellow, Fig. 2*D*). This division held whether the reporter affected primarily the first step of splicing, the second step, or both (Table S2). Differences in the extent of the effect varied with individual *prp8* toggle alleles. For example, V1860D and V1860N both exhibited a hyperaccurate/inefficient phenotype; however, the phenotype was much stronger in *prp8* V1860D regardless of reporter. Such variability is not unexpected,

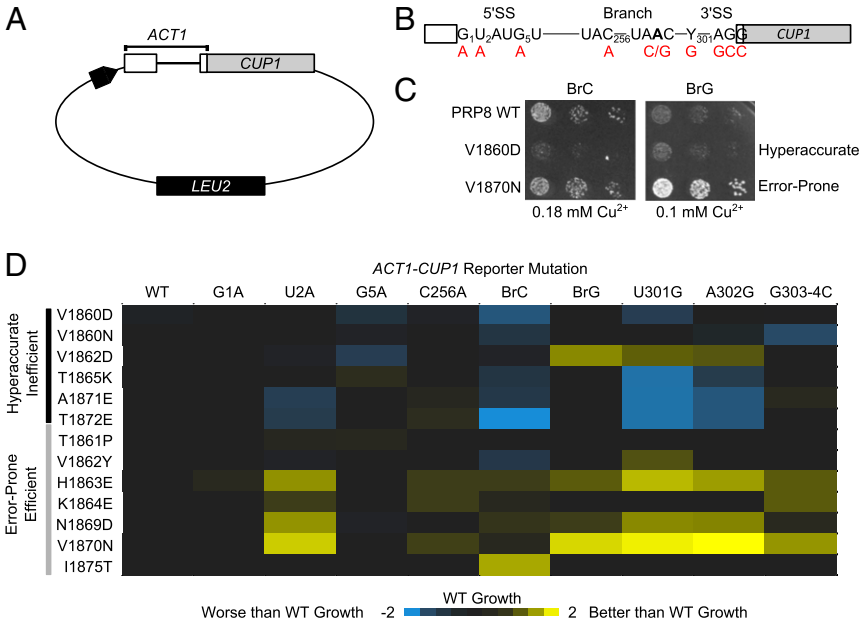

Fig. 2. (*A*) Schematic of *ACT1-CUP1* reporter. (*B*) Diagram of *ACT1-CUP1* reporter intron. The 5′SS, BrA, and 3′SS are shown with mutations made to test fidelity in red. (*C*) Growth of *prp8* toggle alleles in the presence of BrC (*Left*) or BrG (*Right*). (*D*) $[Cu^{2+}{}_{max}]$ that supports growth was determined for each *prp8* toggle allele and reporter. Values were transformed $\log_2([Cu^{2+}{}_{max}\ prp8]/[Cu^{2+}{}_{max}\ PRP8])$ and colored blue (worse growth) to yellow (better growth).

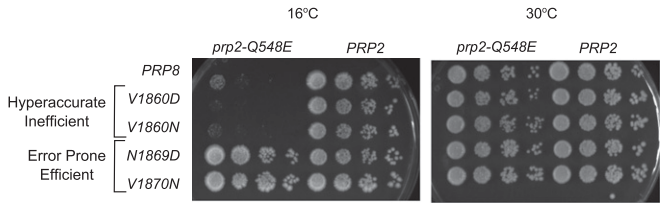

Fig. 3. Growth of double-mutant strains carrying WT, V1860D, V1860N, N1869D, and V1870N *prp8* alleles in combination with *PRP2* or *prp2-Q548E* at 16 °C (*Left*) and 30 °C (*Right*).

because toggle alleles may bias RH domain conformation to differing degrees. These data suggested that *prp8* toggle alleles could be broadly classified as exhibiting hyperaccurate/inefficient or error-prone/efficient splicing, associated with the β-hairpin and loop conformations of the RH extension, respectively.

Toggle Alleles Interact Genetically with an ATPase-Deficient *prp2* Allele. The DEAH-box helicase Prp2 is required for the first catalytic step of splicing (1). Prp2 destabilizes the association between the U2 snRNP and the pre-mRNA before the first step (26) and promotes snRNA rearrangements in preparation for catalysis (27). Strains containing the *prp2*-Q548E allele are impaired for growth at 16 °C and exhibit defects in pre-mRNA splicing, likely due to deficiencies in ATP binding and/or hydrolysis that lead to inefficient catalytic activation (27). We made double-mutant strains that contained *prp2*-Q548E in combination with *prp8* alleles from each class identified in our *ACT1-CUP1* reporter assay: V1860D and V1860N (hyperaccurate/inefficient) and N1869D and V1870N (error-prone/efficient). Hyperaccurate/inefficient *prp8* alleles exhibited synthetic sickness at 16 °C when combined with *prp2*-Q548E whereas error-prone/efficient *prp8* toggle alleles rescued the cold sensitivity of the *prp2*-Q548E strain (Fig. 3). Because Prp2 is required for catalytic activation, these data are consistent with a model in which error-prone/efficient *prp8* alleles promote splicing catalysis whereas hyperaccurate/inefficient oppose it.

In Vitro Characterization of the First-Step Splicing Efficiency of *prp8* Toggle Mutants. To more directly assess first-step splicing efficiency we performed in vitro splicing assays using a splicing substrate truncated just downstream of the branch site. This substrate is unable to complete the second step because it lacks a 3′SS (19, 28), enabling more robust characterization of the first step. Fig. 4*A* shows a representative time-course experiment performed in *PRP8* extract and extracts made from two toggle alleles (V1860D and V1870N) that, based upon *ACT1-CUP1* reporter assays, were expected to have opposite effects on splicing efficiency. Whereas extracts made from error-prone/efficient *prp8* toggle alleles spliced the truncated pre-mRNA with efficiency similar to WT, those from hyperaccurate/inefficient *prp8* alleles exhibited decreased efficiency.

Because the first-step reaction was essentially complete at 10 min (Fig. 4*B*), we repeated this analysis with extracts made from all *prp8* toggle alleles but focused only on the 10-min time point (Fig. 4*C*). On the whole, hyperaccurate/inefficient alleles performed the first step of splicing less efficiently than WT, whereas error-prone/efficient alleles performed the first step with similar or increased efficiency. There were a few exceptions: Three of the *prp8* toggle alleles classified as error-prone/efficient based on *ACT1-CUP1* reporter data (V1862Y, K1864E, and I1875T) spliced with lower efficiency, whereas the hyperaccurate/inefficient *prp8* allele A1871E spliced with efficiency similar to WT. This might reflect allele-specific variability in the artificial context of in vitro splicing with a truncated pre-mRNA and hints at additional complexity in the mode of action of the *prp8* toggle alleles.

To further characterize first-step catalytic efficiency we used extracts made from *prp8* toggle alleles to perform in vitro splicing assays on a full-length *ACT1* pre-mRNA harboring a BrC mutation (Fig. 4*D* and Fig. S2). The BrC mutation decreases the efficiency of both steps, with a particularly strong effect on the first step (17, 29). Extracts from most of the error-prone/efficient *prp8* toggle alleles spliced a BrC-containing substrate more efficiently than *PRP8*. This included extracts from two of the alleles that had spliced the truncated pre-mRNA substrate less efficiently, further indicating potential template-specific effects. All extracts made from hyperaccurate/inefficient *prp8* alleles spliced BrC template less efficiently than WT. Some extracts from both *prp8* toggle allele classes were unable to splice mutant templates in vitro. Because all of the extracts spliced the WT template, we presume that this inefficiency reflects a specific defect between the mutant template and these extracts.

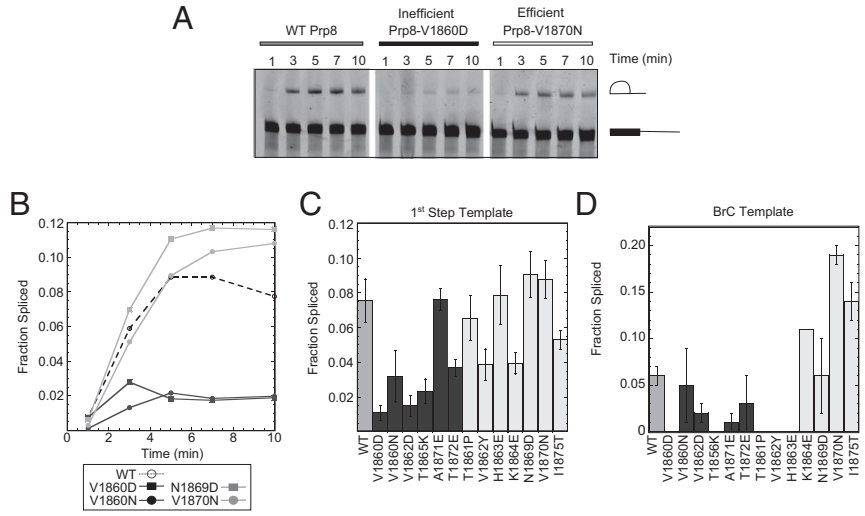

Fig. 4. (*A*) First-step in vitro splicing assay. Gel showing results of a time course of splicing of a fluorescent pre-Act1 truncated template. Pre-mRNA and first-step product indicated. (*B*) Quantification of representative first-step time course assay. (*C*) Fraction truncated pre-Act1 spliced after 10 min. (*D*) Fraction pre-BrC template spliced after 20 min is shown. Hyperaccurate/inefficient alleles colored black, error-prone/efficient gray. Error bars are SEM for three biological replicates.

Lariat Sequencing Reveals Genomewide Alterations to Splicing Fidelity. Given the altered fidelity of *prp8* RH alleles as revealed by reporter constructs, we sought to assess the global impacts of *prp8* RH alleles on the in vivo splice-site selection for native introns. Several groups, including ours, have recently described methods for determining the global locations of splice-site activation by monitoring the lariats generated during each splicing reaction (30–34). Here we developed a modified approach that enables quantitative assessment of splice-site use (*SI Materials and Methods*). Strains were created carrying the *prp8* toggle alleles in combination with a deletion of the *DBR1* gene, an essential component of the lariat decay pathway, to facilitate lariat accumulation. Lariat RNAs were enriched from the total RNA by first depleting the sample of rRNAs and then enzymatically degrading linear RNAs. When cDNA generated from lariat RNAs is subjected to high-throughput sequencing, a subset of sequencing reads that traverse the 2′,5′ linkage can be used to extract the specific 5′SS and Br sequences that were activated in the splicing reaction (32). Although reverse transcriptase exhibits a low propensity to transcribe across the 2′,5′ linkage under standard reaction conditions, here we identified conditions that allow for an ∼100-fold increase in the frequency of read-through (Fig. S3).

We identified the global locations of splice-site activation in WT *PRP8*, as well as in two *prp8* toggle alleles from each of the hyperaccurate/inefficient (V1860D and V1860N) and error-prone/efficient (N1869D and V1870N) classes (Fig. 5). When considering only the WT *PRP8* strain, lariat reads were detected for 287 of the 308 (93%) annotated spliceosomal introns, a level of coverage that exceeded that obtained by other published lariat sequencing approaches in *Saccharomyces cerevisiae* (33, 34) and established the capacity of this approach to readily capture global sites of splicing activation (Fig. S4 and Datasets S1 and S2). Consistent with previous studies, this analysis also revealed use of alternative splice sites associated with known introns (30–34), herein referred to as aberrant splice sites. We focused further analyses on the aberrant events with sufficient read depth across all strains to enable statistical analyses.

For each event, the frequency of aberrant splice-site activation relative to the frequency of annotated splice-site activation was determined for the selected *prp8* toggle alleles. Fig. 5*A* shows a false-colored representation of the behavior of each of these aberrant splicing events relative to *PRP8*. When considering the behavior of the different alleles across all of these splicing events, the behaviors of the pair of hyperaccurate/inefficient alleles highly correlated with one another (Pearson $r = 0.82$), and the behaviors of the pair of error-prone/efficient alleles highly correlated with one another (Pearson $r = 0.87$). By contrast, the behavior of the hyperaccurate/inefficient pairs was poorly correlated with that of the error-prone/efficient pairs (Pearson $r = -0.11$), consistent with these classes of alleles having opposing impacts on these aberrant events. Moreover, when considering the behavior of the individual splicing events in the context of *prp8* toggle alleles, events largely matched the results seen with *ACT1-CUP1* reporters (Fig. 2 and Fig. S1) wherein the hyperaccurate/inefficient alleles showed lower levels of aberrant splice-site activation than the WT, while the error-prone/efficient alleles showed higher levels. As with the reporters, the level of aberrant splice-site activation varied with the different *prp8* toggle alleles.

To independently validate the frequencies of specific aberrant splice-site activation events determined from lariat sequencing, we used a PCR-based approach to quantify the different lariat species (Fig. S5). As seen in Fig. 5*B*, primers were designed such that they faced away from one another in the context of linear RNA but toward one another in the context of a lariat. The amplicons derived from these primer pairs differed in length depending upon the particular 5′SS used in the reaction, allowing the relative abundancies of the two isoforms to be determined by capillary electrophoresis on a Bioanalyzer. The results of these experiments were largely consistent with lariat sequencing results (Fig. 5 *C*–*E*). Decreased levels of aberrant splice-site activation were apparent in the hyperaccurate/inefficient alleles relative to WT, with the strongest phenotypes apparent in both assays for the V1860D mutant, consistent with our observations on *ACT1-CUP1* reporters. The effects of the error-prone/efficient alleles were more modest, showing subtle yet consistent increases in the use of aberrant splice sites within some of the transcripts and little change from WT within others.

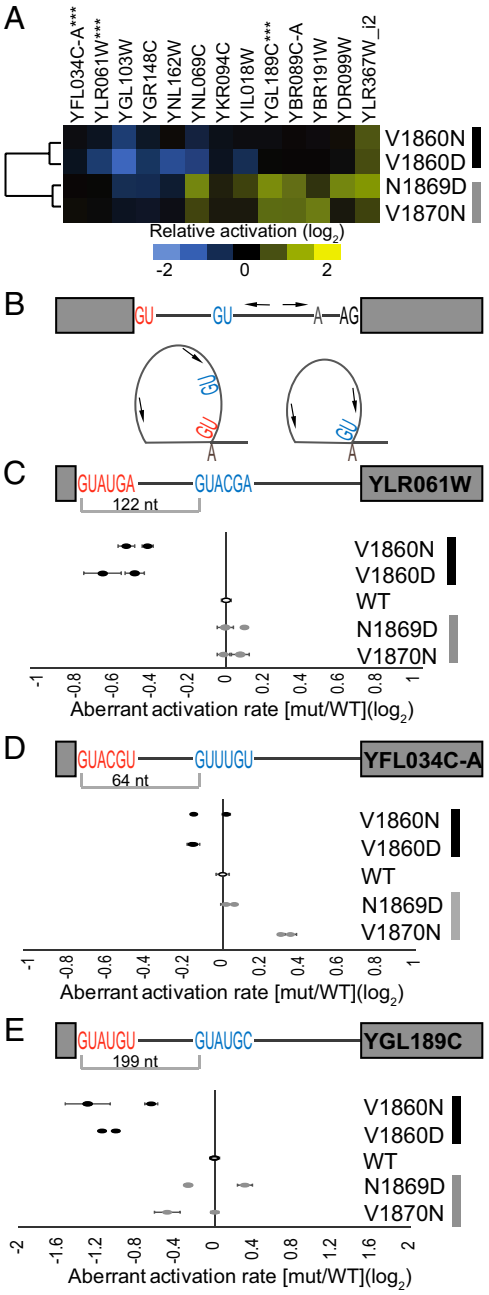

Fig. 5. (*A*) Global lariat sequencing identified specific locations of increases (yellow) and decreases (blue) in aberrant 5′SS activation associated with annotated introns. (*B*) Schematic of primer locations (arrows) that enable discrimination between annotated (red) and aberrant (blue) splice-site activation (Table S4). (*C*–*E*) Relative splice-site use as determined by RT-PCR is shown for two biological replicates of each strain. Hyperaccurate/inefficient alleles colored black, error-prone/efficient gray. Error bars are SD for two technical replicates.

Discussion

Here we present an analysis of the role of the RNaseH domain (RH) of Prp8 in spliceosomal activity. Specifically we reveal two classes of mutants in the RH extension of Prp8, transitional (inefficient/hyperaccurate) and catalytic (efficient/error-prone). Furthermore, because these transitional and catalytic *prp8* alleles stabilize mutually exclusive β-hairpin and loop conformations of the RH extension of Prp8 (Fig. 1 and Table S1) (19), our data directly link a conformational change in the spliceosome to genomewide changes in splicing fidelity.

The Toggle Model. We suggest that the RH extension of Prp8 is a structural toggle, oscillating between mutually exclusive conformations at distinct points in the splicing cycle to promote high-fidelity, high-efficiency splicing. Specifically, we propose that the RH extension adopts the transitional conformation before the first step, toggles to the catalytic for the first step, toggles back to the transitional between catalytic steps, and then again adopts the catalytic conformation for the second step—a "toggle model" (Fig. 6). That the RH extension adopts the catalytic form at both catalytic steps is supported by growth assays where yeast expressing catalytic *prp8* alleles promote the splicing of a variety of *ACT1-CUP1* reporters in vivo, regardless of which catalytic step is affected by the reporter (Fig. 2 and Fig. S2) (13, 16–19), our in vitro splicing assays (Fig. 4), and the structure of a B^{act} spliceosome (5). That RH adopts a transitional form before the first and again between the first and second steps is supported by structures of C and C* spliceosomes (7, 8, 10, 11) and by genetic interactions between *prp8* toggle alleles and the DEAH-box ATPases Prp2 and Prp16, which promote spliceosome conformational changes required for the first and second steps. Catalytic *prp8* alleles suppress growth defects in yeast expressing ATPase-deficient Prp2, whereas transitional *prp8* alleles exacerbate them (Fig. 3). These same catalytic alleles also suppress the growth defect of yeast expressing ATPase-deficient Prp16 (17, 18).

The biological relevance of conformational toggling is well understood for the ribosome, another large, high-fidelity RNP machine that shares numerous similarities with the spliceosome (2). The ribosome repeatedly moves between "open" and "closed" conformations. Proofreading, which allows for the rejection of a near-cognate tRNA, takes place in the open state, whereas peptide bond catalysis occurs in the closed (35). Translational fidelity and ribosome conformation have been directly linked through studies of ribosome mutants known as ribosomal ambiguity (*ram*) and restrictive. *Ram* mutants favor the closed, catalytic form of the ribosome and destabilize the proofreading conformation, even in the presence of near-cognate tRNA, resulting in coding errors and more rapid translation. Restrictive mutants have the opposite effect: They favor the open, proofreading conformation and are hyperaccurate (35).

The first-step/second-step model was proposed in 2004 and was the first spliceosomal model to invoke conformational toggling by the ribosome (17). By this model the spliceosome alternates between unique first- and second-step conformations (13, 17–19, 36) wherein first- and second-step alleles of *prp8* bias the conformation of the spliceosome toward first- or second-step conformations, respectively. Primer extensions performed on *ACT1-CUP1* reporter RNA isolated from strains carrying first- and second-step alleles were key to the development of this model. However, for the subset of *prp8* alleles that map to the RH extension, we note that these data are also consistent with the toggle model. Rather than a preference to dwell in a second-step conformation, decreased lariat intermediate and increased mRNA levels exhibited by second-step alleles can also indicate more rapid progression through both steps of splicing, as we propose. Similarly, instead of a bias toward a first-step conformation, decreased pre-mRNA and increased lariat intermediate levels observed in first-step alleles are consistent with a general bias against catalysis; the limited number of spliceosomes that succeed at the first step are unable to complete the second.

The RH domain of Prp8 is not the only spliceosomal component that toggles. Stem II of the U2 snRNA can fold into two mutually exclusive structures: Stem IIa and Stem IIc (37, 38). Alleles that bias toward the Stem IIa conformation have fidelity phenotypes similar to *prp8* transitional alleles. These alleles also have genetic and proofreading phenotypes comparable to *prp16* ATPase-deficient alleles. In contrast, the U2 Stem IIc conformation has been shown to be necessary for both catalytic steps. Alleles that promote the U2 Stem IIc conformation have phenotypes similar to the *prp8* catalytic alleles, as do mutations within the myb-domain of Cef1 (36–38). We speculate that these individual toggles might be linked; the spliceosome as a whole may toggle between catalytic and transitional conformations.

Conclusion. Although the ribosome and spliceosome are separated by billions of years of evolution, they exhibit many similarities including our demonstration here of a direct coupling of catalytic efficiency with fidelity. Whereas work over the past decade has shed light on the mechanisms by which structural changes in the ribosome enable discrimination of cognate from near-cognate tRNAs, we have only begun to investigate these mechanisms in the spliceosome, owing at least in part to the difficulty in determining whether a splice site should be considered as "cognate" or "near-cognate." In fact, in the current work probing budding yeast, where splice sites have evolved to conform to a precise consensus sequence, the global locations of aberrant splice-site activation are marked by splice-site sequences that in many instances look far more cognate than do many annotated mammalian splice sites (Fig. 5 *C–E*). Nevertheless, there are many more locations across the genome where strong potential splice sites exist yet for which we

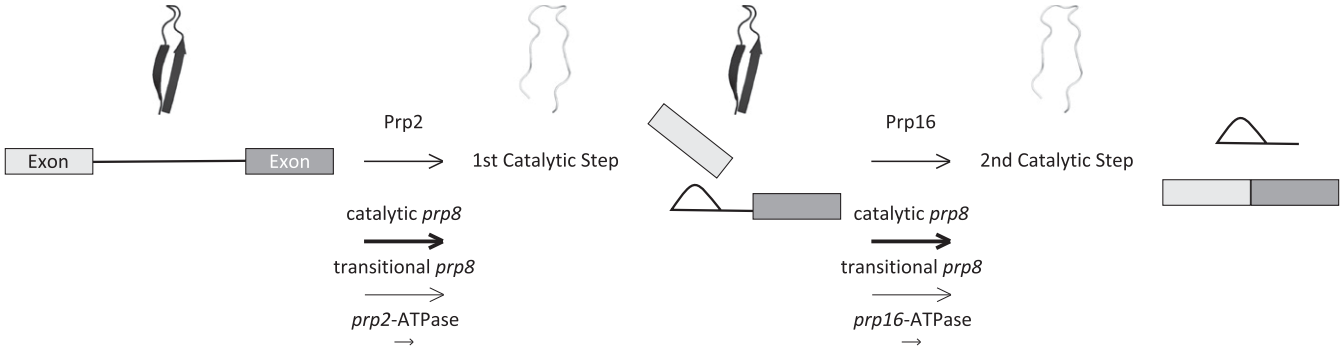

Fig. 6. The toggle model. The Prp8 RH extension toggles between catalytic (error-prone/efficient) and transitional (hyperaccurate/inefficient) forms during the splicing cycle. Prp2 ATPase activity promotes the first catalytic step; Prp16 ATPase activity promotes the second. Catalytic *prp8* toggle alleles bias the spliceosome toward the catalytic conformation at both the first and second steps, whereas transitional mutants bias against conversion to the catalytic conformation.

detect no activation. Understanding why the spliceosome activates some of these sites but not others will be key to understanding the relationship between catalytic efficiency and fidelity on the spliceosome. Likewise, it will be crucial to identify structural conformations of the spliceosome that can trigger the interconversion between proofreading and catalytic states, which could contribute to alternative splice-site selection in higher organisms.

Materials and Methods

Standard molecular biology and genetic techniques were used as described previously (24, 25, 39) and are detailed in *SI Materials and Methods*. Table S3 contains a list of strains used in this work. Plasmids are available through Addgene (www.addgene.org).

For lariat sequencing, enrichment of lariat RNAs from total cellular RNA was accomplished by an initial treatment with Illumina's Ribo-Zero Gold rRNA Removal Kit (yeast), followed by treatment with RNaseR at 37 °C for 10 min to digest the linear species. First-strand cDNA synthesis was performed on the remaining RNA under otherwise standard conditions but where $MgCl_2$ was replaced with 3 mM $MnCl_2$ to facilitate read-through of the 2′,5′ lariat bond. Libraries for sequencing were generated as previously described (32). A detailed protocol is provided in *SI Materials and Methods*. Lariat sequencing data can be accessed from the NCBI GEO database (accession no. GSE96891).

ACKNOWLEDGMENTS. We thank D. Velazquez, A. de Bruyn Kops, K. Patrick, Y. He, Z. Dwyer, and M. Dinglasan for help with experiments and the J. Staley, C. Query, and M. Konarska laboratories for strains and plasmids. We thank J. Burke and H. Madhani for helpful discussions. This work was supported by NIH Grants R01GM2119-42 (to C.G.) and R01GM098634 (to J.A.P.) and a Research Scholar Grant from the American Cancer Society (to J.A.P.). C.G. is an American Cancer Society Research Professor of Molecular Genetics.

1. Wahl MC, Will CL, Lührmann R (2009) The spliceosome: Design principles of a dynamic RNP machine. *Cell* 136:701–718.
2. Semlow DR, Staley JP (2012) Staying on message: Ensuring fidelity in pre-mRNA splicing. *Trends Biochem Sci* 37:263–273.
3. Nguyen THD, et al. (2016) Cryo-EM structure of the yeast U4/U6.U5 tri-snRNP at 3.7 Å resolution. *Nature* 530:298–302.
4. Wan R, et al. (2016) The 3.8 Å structure of the U4/U6.U5 tri-snRNP: Insights into spliceosome assembly and catalysis. *Science* 351:466–475.
5. Rauhut R, et al. (2016) Molecular architecture of the Saccharomyces cerevisiae activated spliceosome. *Science* 353:1399–1405.
6. Yan C, Wan R, Bai R, Huang G, Shi Y (2016) Structure of a yeast catalytically activated spliceosome at 3.5 Å resolution. *Science* 353:904–11.
7. Galej WP, et al. (2016) Cryo-EM structure of the spliceosome immediately after branching. *Nature* 537:197–201.
8. Wan R, Yan C, Bai R, Huang G, Shi Y (2016) Structure of a yeast catalytic step I spliceosome at 3.4 Å resolution. *Science* 353:895–904.
9. Yan C, et al. (2015) Structure of a yeast spliceosome at 3.6-angstrom resolution. *Science* 349:1182–1191.
10. Bertram K, et al. (2017) Cryo-EM structure of a human spliceosome activated for step 2 of splicing. *Nature* 542:318–323.
11. Fica SM, et al. (2017) Structure of a spliceosome remodelled for exon ligation. *Nature* 542:377–380.
12. Grainger RJ, Beggs JD (2005) Prp8 protein: At the heart of the spliceosome. *RNA* 11:533–557.
13. Yang K, Zhang L, Xu T, Heroux A, Zhao R (2008) Crystal structure of the beta-finger domain of Prp8 reveals analogy to ribosomal proteins. *Proc Natl Acad Sci USA* 105: 13817–13822.
14. Kuhn AN, Brow DA (2000) Suppressors of a cold-sensitive mutation in yeast U4 RNA define five domains in the splicing factor Prp8 that influence spliceosome activation. *Genetics* 155:1667–1682.
15. Kuhn AN, Reichl EM, Brow DA (2002) Distinct domains of splicing factor Prp8 mediate different aspects of spliceosome activation. *Proc Natl Acad Sci USA* 99:9145–9149.
16. Collins CA, Guthrie C (1999) Allele-specific genetic interactions between Prp8 and RNA active site residues suggest a function for Prp8 at the catalytic core of the spliceosome. *Genes Dev* 13:1970–1982.
17. Query CC, Konarska MM (2004) Suppression of multiple substrate mutations by spliceosomal prp8 alleles suggests functional correlations with ribosomal ambiguity mutants. *Mol Cell* 14:343–354.
18. Liu L, Query CC, Konarska MM (2007) Opposing classes of prp8 alleles modulate the transition between the catalytic steps of pre-mRNA splicing. *Nat Struct Mol Biol* 14:519–526.
19. Schellenberg MJ, et al. (2013) A conformational switch in PRP8 mediates metal ion coordination that promotes pre-mRNA exon ligation. *Nat Struct Mol Biol* 20:728–734.
20. Siatecka M, Reyes JL, Konarska MM (1999) Functional interactions of Prp8 with both splice sites at the spliceosomal catalytic center. *Genes Dev* 13:1983–1993.
21. Fica SM, et al. (2013) RNA catalyses nuclear pre-mRNA splicing. *Nature* 503:229–234.
22. Marcia M, Pyle AM (2012) Visualizing group II intron catalysis through the stages of splicing. *Cell* 151:497–507.
23. Umen JG, Guthrie C (1996) Mutagenesis of the yeast gene PRP8 reveals domains governing the specificity and fidelity of 3′ splice site selection. *Genetics* 143:723–739.
24. Lesser CF, Guthrie C (1993) Mutational analysis of pre-mRNA splicing in Saccharomyces cerevisiae using a sensitive new reporter gene, CUP1. *Genetics* 133:851–863.
25. Mayerle M, Guthrie C (2016) Prp8 retinitis pigmentosa mutants cause defects in the transition between the catalytic steps of splicing. *RNA* 22:798–809.
26. Ohrt T, et al. (2012) Prp2-mediated protein rearrangements at the catalytic core of the spliceosome as revealed by dcFCCS. *RNA* 18:1244–1256.
27. Wlodaver AM, Staley JP (2014) The DExD/H-box ATPase Prp2p destabilizes and proofreads the catalytic RNA core of the spliceosome. *RNA* 20:282–294.
28. Anderson K, Moore MJ (2000) Bimolecular exon ligation by the human spliceosome bypasses early 3′ splice site AG recognition and requires NTP hydrolysis. *RNA* 6:16–25.
29. Fouser LA, Friesen JD (1986) Mutations in a yeast intron demonstrate the importance of specific conserved nucleotides for the two stages of nuclear mRNA splicing. *Cell* 45:81–93.
30. Taggart AJ, DeSimone AM, Shih JS, Filloux ME, Fairbrother WG (2012) Large-scale mapping of branchpoints in human pre-mRNA transcripts in vivo. *Nat Struct Mol Biol* 19:719–721.
31. Awan AR, Manfredo A, Pleiss JA (2013) Lariat sequencing in a unicellular yeast identifies regulated alternative splicing of exons that are evolutionarily conserved with humans. *Proc Natl Acad Sci USA* 110:12762–12767.
32. Stepankiw N, Raghavan M, Fogarty EA, Grimson A, Pleiss JA (2015) Widespread alternative and aberrant splicing revealed by lariat sequencing. *Nucleic Acids Res* 43:8488–8501.
33. Gould GM, et al. (2016) Identification of new branch points and unconventional introns in Saccharomyces cerevisiae. *RNA* 22:1522–1534.
34. Qin D, Huang L, Wlodaver A, Andrade J, Staley JP (2016) Sequencing of lariat termini in S. cerevisiae reveals 5′ splice sites, branch points, and novel splicing events. *RNA* 22:237–253.
35. Ogle JM, Murphy FV, Tarry MJ, Ramakrishnan V (2002) Selection of tRNA by the ribosome requires a transition from an open to a closed form. *Cell* 111:721–732.
36. Query CC, Konarska MM (2012) CEF1/CDC5 alleles modulate transitions between catalytic conformations of the spliceosome. *RNA* 18:1001–1013.
37. Hilliker AK, Mefford MA, Staley JP (2007) U2 toggles iteratively between the stem IIa and stem IIc conformations to promote pre-mRNA splicing. *Genes Dev* 21:821–834.
38. Perriman RJ, Ares M, Jr (2007) Rearrangement of competing U2 RNA helices within the spliceosome promotes multiple steps in splicing. *Genes Dev* 21:811–820.
39. Guthrie C, Fink GR, eds (2004) *Guide to Yeast Genetics and Molecular and Cell Biology* (Elsevier, London).
40. Price AM, Görnemann J, Guthrie C, Brow DA (2013) An unanticipated early function of DEAD-box ATPase Prp28 during commitment to splicing is modulated by U5 snRNP protein Prp8. *RNA* 20:40–60.
41. Edwalds-Gilbert G, et al. (2000) Dominant negative mutants of the yeast splicing factor Prp2 map to a putative cleft region in the helicase domain of DExD/H-box proteins. *RNA* 6:1106–1119.
42. Collins CA, Guthrie C (2001) Genetic interactions between the 5′ and 3′ splice site consensus sequences and U6 snRNA during the second catalytic step of pre-mRNA splicing. *RNA* 7:1845–1854.